Qeios

Deep Learning Modeling for Prediction of Cognitive Task Related Features from Resting-state fMRI Data

Takaki Tokuhiro, Keiichi Onoda, Masahiro Takamura, Shuhei Yamaguchi, Hiroyuki Akama

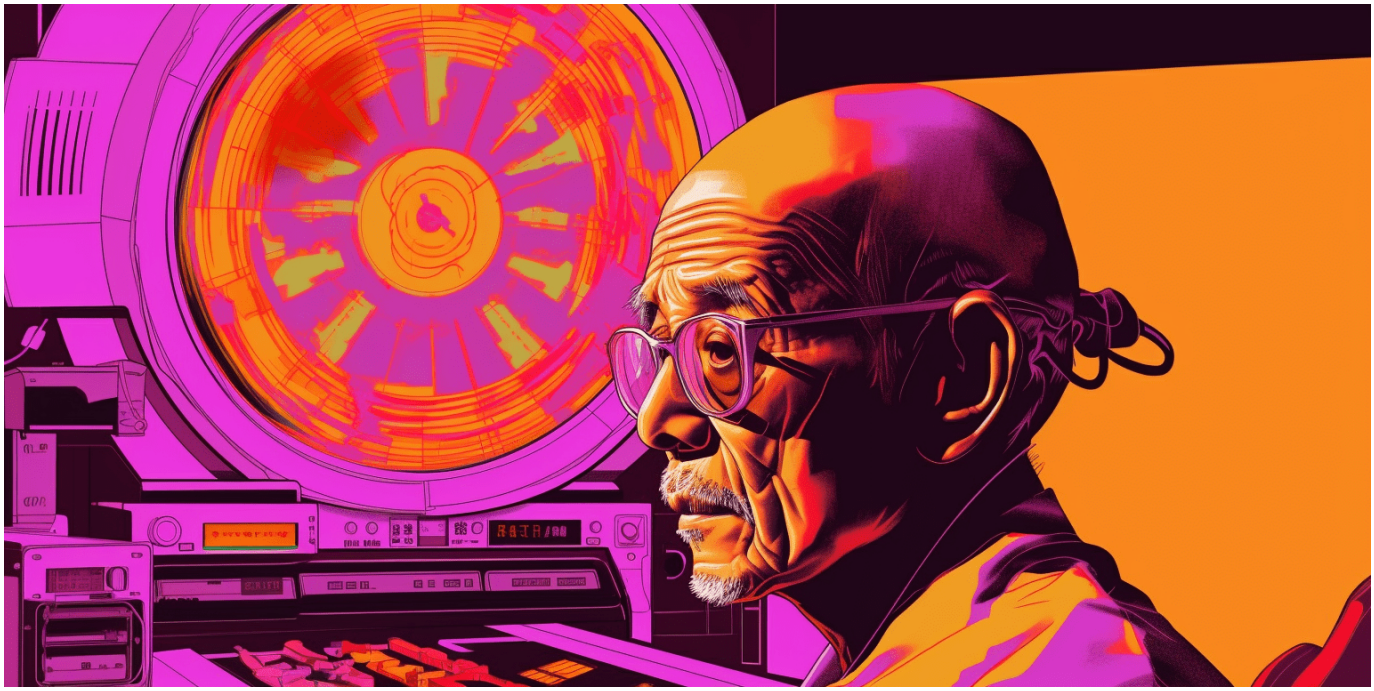

v1

June 8, 2023

https://doi.org/10.32388/GDWCBK

Deep Learning Modeling for Prediction of Cognitive Task Related Features from Resting-state fMRI Data

Takaki Tokuhiro[1], Keiichi Onoda[2], Masahiro Takamura[3], Shuhei Yamaguchi[4], Hiroyuki Akama[5,6*]

1 Ex-School of Life Science and Technology, Tokyo Institute of Technology, Tokyo, Japan (Alumnus); 2 Faculty of Psychology, Otemon Gakuin University, Osaka, Japan; 3 Faculty of Medicine, Shimane University, Shimane, Japan; 4 Department of Neurology, Shimane Prefectural Central Hospital, Shimane, Japan; 5 School of Life Science and Technology, Tokyo Institute of Technology, Tokyo, Japan; 6 Institute of Liberal Arts, Tokyo Institute of Technology, Tokyo, Japan

* Corresponding author

Abstract

In recent years, several neural network methods, such as brain functional networks, have been proposed to efficiently learn non-Euclidean graph structures. In this study, we modified the connectivity-based graph convolutional network (cGCN) developed by Wang et al. (2021) for autism spectrum disorder (ASD) classification into a regression model and used resting-state functional magnetic resonance imaging (rs-fMRI) data to predict the scores on the offline Kohs block-design test for a total of 615 subjects aged 33–89 years. To convert from discrimination to regression, we employed a technique that introduces a fully connected layer in the cGCN and connects the long short-term memory (LSTM) in the last output phase instead of the Softmax layer. The results showed that our cGCN–LSTM was more accurate than the baseline LASSO regression model, and that the predictions correlated significantly with the measured scores of the cognitive function test. Moreover, we used the leave-one-out and leave-two-out occlusion methods to extract important regions of interest (ROIs), as well as networks from the

model. It was acknowledged that the Kohs block-design test scores were negatively correlated with age, but the results suggested the possibility of age-related cognitive decline that could not be captured by age prediction models alone. We found that only the nodes of the default mode network and cerebellum contain some significant within-networks; however, overall, between-network connectivity overwhelmingly contributed to the prediction regardless of the weight of the role in the age projection. This model and the leave-two-out occlusion method allowed us to identify the regions and networks involved in further task-based fMRI experiments in advance. Our methodology has the potential to make the design of task fMRI experiments more rational and accurate before planning and conducting actual scans.

Keywords: fMRI, Kohs block-design test, score prediction, cGCN, LSTM

1. Introduction

In neuroimaging research, a brain connectome called resting-state functional connectivity (rs-FC) is being investigated using functional magnetic resonance imaging (fMRI) to provide a neural basis for cognitive abilities and biomarkers for neurological diseases. It does not require a specific task and can be applied to subjects of all ages, ranging from infants to the elderly. It is also relatively easy to scale across imaging sites, and a large amount of data is readily available. Because of these advantages, rs-FC is highly compatible with recent machine-learning-based disease diagnoses and age prediction. When explanatory variables are selected from brain imaging data and subject attributes are set as objective variables, a common regression or discriminant analysis approach is utilized to solve a binary or multivalued classification problem regarding the subject attributes; this can aid diagnosis in clinical settings using biomarkers. However, predicting a participant's test scores with respect to task-related cognitive functions or score regression is generally considered challenging. This is especially true when predicting complex offline executive control performance from resting-state data alone, which are recorded using a magnetic resonance imaging (MRI) scanner. However, given that default mode network (DMN) connectivity decreases with

cognitive decline, rs-FC can be used as an indicator of cognitive decline and psychiatric disorders. In particular, a model that predicts cognitive test scores that decrease with age can be utilized to deduce persons' cognitive abilities even if the input data are the same, thus emphasizing its practical versatility. In addition, by analyzing the internal mechanisms of individual prediction models for different tasks, it is possible to explore the brain regions and functional networks that have different and important effects on various cognitive abilities.

Studies predicting cognitive test scores from resting-state fMRI (rs-fMRI) are less common than those implementing discriminative modeling of neurological disorders such as Alzheimer's disease (AD). Meskaldji et al., 2016a calculated functional connectivity (FC) from rs-fMRI and used partial least squares regression (PLSR) to predict the scores on the long-term memory test for 57 subjects with mild cognitive impairment (MCI); correlation coefficients between actual and predicted scores ranged within 0.417–0.646. DMN regions such as the hippocampus, superior frontal lobe, and temporal lobe were found to be important for prediction. Subsequently, Meskaldji et al., 2016b used PLSR to predict episodic memory capacity with correlation coefficients ranging within 0.53–0.64, and found that the DMN, sensorimotor network (SMN), limbic system, and bilateral supplementary motor areas were important regions of interest (ROIs). Other relevant research includes the prediction of clinical measures of depression using PLSR (Yoshida et al., 2017) and of intelligence quotient (IQ) scores from rs-FC using the graph neural network (GNN) model (Hanik et al., 2022); the results of these studies suggest that an individual's rs-FC contains important behavioral and clinical information. Based on this previous research, this study investigates the relationship between rs-FC and cognitive functions that change with age by predicting task test scores from rs-FC. We followed but slightly modified the connectivity-based graph convolutional network (cGCN) of Wang et al., 2021 from discrimination to regression. Thus, we predicted the values of the Kohs block-design test (Kohs, 1920) using data from the Brain Dock records of 695 participants at the Shimane Institute of Health Science (Minowa et al., 2022). The scores of this test are negatively correlated with age, making them the best indicators of age-related cognitive decline. Therefore, it was required to regress the effects of age as an important factor.

2. Materials and Methods

2.1 Participants

For the MRI participants, data acquisition, and preprocessing, the datasets and the procedures were identical to those of our previous study, Minowa et al., 2022. We analyzed 333 male and 282 female healthy participants, of which the age composition is the following: 37 subjects aged 30–39, 97 aged 40–49, 107 aged 50–59, 156 aged 60–69, 166 aged 70–79, and 52 aged 80–89 (mean age: 62.4 ± 13.5 years). The dataset is characterized by the fact that it is a periodic examination of primarily old, healthy subjects without neurological diseases, given that the correlation between the motivation score, called the Apathy score, and age is relatively small (-0.137), suggesting that many subjects are particularly healthy for their age.

2.2 MRI data

MRI data were acquired using a Philips Ingenia 3.0T scanner which was installed at the Shimane Institute of Health Science in 2016. The total duration of the rs-fMRI scans for each participant was 350 s, with the following parameters: repetition time (TR) = 2500 ms, echo time (TE) = 30 ms, field of view (FOV) (right-left (RL) = 212 mm, anterior-posterior (AP) = 212 mm, feet-head (FH) = 159.2 mm), acquisition (ACQ) matrix M × P = 64 × 63, number of slices = 40, and slice thickness = 3.2 mm. After converting the DICOM data into NIfTI images using the dcm2niix DICOM to NIfTI converter (The Neuropsychology Lab, University of South Carolina, SC, USA), we preprocessed the images via the Configurable Pipeline for the Analysis of Connectomes (Craddock et al., 2013) using the default configuration of version 1.7.0. ROI-mean time series data were computed from Automated Anatomical Labeling (AAL, Tzourio-Mazoyer et al., 2002) and normalized using the method *ConnectivityMeasure* provided by the nilearn.connectome application programming interface (API) (Abraham et al., 2014). In this library, the population variance and covariance matrices were estimated using the Ledoit–Wolf method and the population correlation matrix was calculated. The group average FC was obtained by averaging the FC matrix for all

subjects. At this time, only training and validation data were used to obtain the group FC to prevent information leakage from the test data. All code used in this study is available to the public at https://github.com/tokuotsu/cGCN-LSTM.git.

2.3 Kohs block-design test

The Brain Dock dataset has several test scores pertaining to neural and cognitive decline, which are prevalent in elderly people. However, in this study, we addressed the results of the Kohs' block-design test (the cube combination test). This intelligence test involving the matching of puzzle patterns was first published by Kohs in 1920. Seventeen tasks are scored based on the time required for each task, with a maximum possible score of 131 points. The mental age (MA) is calculated based on the score using a conversion table and combined with the calendar age (CA); the intelligence quotient (IQ) can be calculated using the following formula:

$$IQ = \frac{MA}{CA} \times 100$$

2.4 Prediction modeling

2.4.1 cGCN regression

In this study, we customized the cGCN developed by Wang et al., 2021, to perform cognitive index prediction. Features that differ from the original model include the use of long short-term memory (LSTM) in the final layer to extract time-series features. An overview of this process is shown in Figure 1.

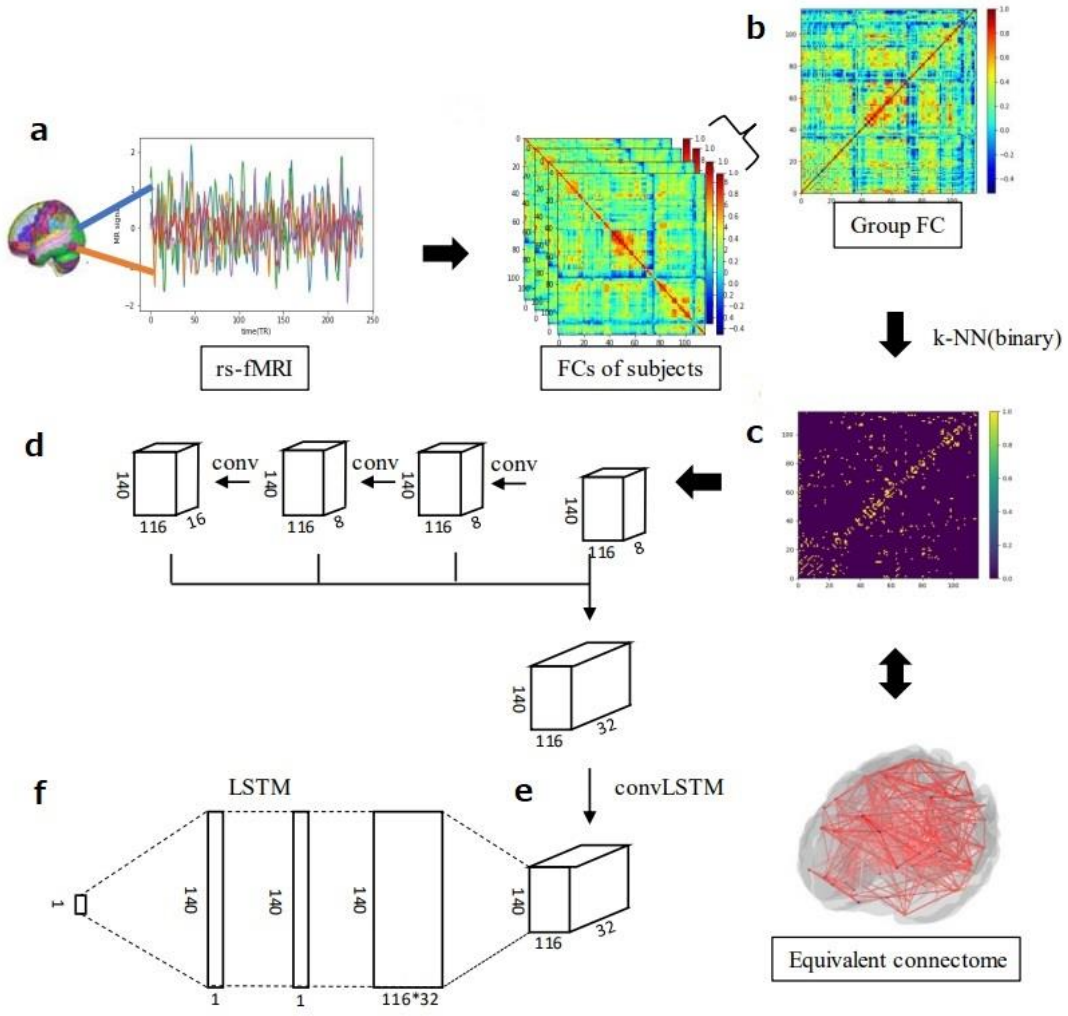

Figure 1. Overall model flow of the proposed cGCN-LSTM. The values at the cubes' sides represent the number of frames (140), the number of ROIs (116), and the number of channels (depth); the fourth dimension is omitted. In this flow, **a,** FC is calculated from the subject's rs-fMRI and **b,** group average FC is computed using only the training data. **c,** The group average FC is obtained by leaving the five nearest neighbors of each ROI, masking them by binarization. **d,** Graph convolution was performed in those ROIs, and **e,** the outputs are passed through convolution to convLSTM. **f,** As the last step, our own LSTM layer is added to obtain the final value (the implementation is our originality to remodel the cGCN by Wang et al., 2021.)

Graph representations were obtained from the group mean FC using the k-nearest neighbor algorithm (k-NN). Specifically, the five representations with the

largest correlation coefficients were selected for each of the 116 AAL areas; the reason for selecting five was that, according to the results of Wang et al., 2021, the accuracy of ASD classification was the highest at k=5 and did not improve beyond that. The same k-NN graph was used across subjects; in the adjacency matrix of the binary graph in a heat map style (Figure 1-c), the bright cells indicate the five nearest neighbors of each area (row). The edges in the brain image below are the visualized networks equivalent to the binary graph.

Next, we explain the graph convolution based on the procedures by Wang et al. 2021, in Figure 1. The dimensions are shown using rectangles, where 140 of these graphics represent the time series (TR), 116 represent the areas of the AAL (ROI), and 8 represent the number of channels. In addition, there is a fourth dimension used for inputting age values but is omitted in this figure. For graph convolution, the following equation is obtained:

$$x_i = \max_{j:(i,j)\in\epsilon} h_\Theta(x_i|x_j - x_i),$$

where x_i represents the blood-oxygen-level-dependent (BOLD) signal of the i^{th} ROI, and x_j represents the BOLD signal of the ROI adjacent to x_i. We limited the number of x_j to five. The signal values x_i and $x_j - x_i$ are input into the two-dimensional convolution described here as h_Θ, and the one with the maximum activity among the outputs is adopted. We introduced skip connections by setting up these convolutions separately, assigning one to be used as an input to the next convolution and the other to be used as is, and combining them later. Skip connections, as in the case of U-Net (De Luca et al., 2006), transmit even low-level features without gradient loss and bypass the previous layer without modification.

The mean squared error (MSE) was used as the loss function in this model with a batch size of 16 and a maximum number of epochs of 200. Learning was performed using the MSE loss; if this did not decrease over 30 epochs, training was terminated at an early stop.

$$MSE(y,\hat{y}) = \frac{1}{n}\sum_{i=1}^{n}(y_i - \hat{y}_i)^2$$

,

where y_i denotes the observed value and $\hat{y}_i$ the predicted value. The final evaluation was performed using Pearson's product-moment correlation coefficient r and the coefficient of determination $R^2(y, \hat{y})$ of the actual and predicted values. Each is defined as follows:

$$r_{xy} = \frac{\sum_{i=1}^{n}(x_i - \bar{x})(y_i - \bar{y})}{\sqrt{\sum_{i=1}^{n}(x_i - \bar{x})^2}\sqrt{\sum_{i=1}^{n}(y_i - \bar{y})^2}}$$

,

$$R^2(y, \hat{y}) = 1 - \frac{\sum_{i=1}^{n}(y_i - \hat{y}_i)^2}{\sum_{i=1}^{n}(y_i - \bar{y})^2},$$

where $\bar{x}$ and $\bar{y}$ are the mean values of x *and* y, respectively. Note that the coefficient of determination has a maximum value of 1, and can be a negative value, as defined.

The model was built using the Keras API, and training was performed using two RTX1080Ti graphic processing units. To prevent leakage of the test data, all data were divided into three subsets at a training: validation: testing ratio of 3:1:1 using 5-fold cross-validation (CV), and the final evaluation was performed using test data not used in the training phase. As mentioned previously, the group-mean FC was estimated from the training and validation data.

The above model followed the original model of Wang et al., 2021, to a large extent, but with the major change being the incorporation of LSTM in the final layer to modify the model from classification to regression. This is because the classification model for autistic patients in Wang et al., 2021, must be converted to a cognitive function score regression model in the present study. For the original model, convolution was performed separately on all time series, and their outputs were averaged as the final result. The inability to directly set a fully connected layer in the network architecture for regression was due to the specification of the existing Tensorflow-gpu==1.4 library; this may be why that type of layer was not used in the implementation of Wang et al., 2021. In the original GCN for classification, averaging of each time series was performed using the recurrent neural network (RNN) in the temporal pooling layer, convLSTM, before being passed on to the final softmax layer. Alternatively, we incorporated an entire network of LSTM in the form of cGCN-LSTM for all joins at the last stage instead of using the softmax function. Therefore, the final

result could be obtained through additional learning, including average computation, to clarify the issue of setting dense connections. Thus, by connecting to a new LSTM, time-series features could be extracted through the fully connected layer such that the regression process can be achieved, as in the case of age prediction with RNNs. The procedures with parameter settings for the cGCN-LSTM are shown in Figure A of the Supplementary Materials.

2.4.2 LASSO regression

We used least absolute shrinkage and selection operator (LASSO) regression as the baseline model and whole-brain functional connectivity strength (FCS) as the feature; FCS is the sum of connection strengths above a threshold value known as weighted order centrality. A node with a high FCS value can be considered a functional hub for a large network (Buckner et al., 2008). Li et al., 2020 also reported that changes in the FCS in the left precuneus are associated with age-related cognitive decline. In the present study, the threshold for calculating the FCS was set at 0.2 based on Li et al., 2020, and the correlation coefficients larger than the threshold were summed for each area, which was used as input information for the LASSO regression. In addition, a 5×5 nested CV was performed to reduce bias in each training dataset and to perform a hyperparameter search simultaneously. In this CV, the hyperparameter α, which determines the strength of regularization in the inner loop, was varied from 10^{-5} to 1 in 100 steps. The final results were obtained by training the entire inner loop using the parameter with the highest accuracy, and making predictions based on the outer test data that were not used for training. Shuffling was performed at random with the same seed as the cGCN five times in the outer loop, allowing for model-to-model comparisons.

2.5 Occlusion methods

The interpretation of models in machine learning, particularly in deep learning, remains an open problem. In this study, we used a method called *occlusion* to extract important ROIs in the model. We determined the ROIs that were important for prediction by taking each of the 116 areas in the AAL atlas, setting the mean time series

in each area (ROI) to zero, and sequentially alternating the input to the learned model with the data containing the missing parts. When excluded from the modeling, the ROI resulting in the largest decrease in prediction accuracy was considered the most important in the prediction model. Moreover, in the current study, we decided to obtain the impact of losing an edge by excluding two ROIs simultaneously. This method has not been used in previous studies and may be crucial for visualizing and evaluating the interiors of deep learning models, which are considered difficult to evaluate. The effect of this leave-two-out occlusion method, particularly in our cGCN-LSTM model, is that the time-series changes in the two ROIs are eventually incorporated into the result output at the fully connected layer, thereby reflecting some interaction between them. Furthermore, if the two ROIs are coupled in a close functional relationship, that is, they are included in a k-NN cluster with k=5, the graph convolution will include the spatial and temporal characteristics of the two ROIs, which can further reflect this interaction.

3. Results

3.1 Predictive results of the Kohs block-design test

Figure 2 shows the observed Kohs block-design test scores on the horizontal axis and the predicted scores on the vertical axis, with the LASSO results indicated by black crosses and the cGCN-LSTM results by red circles. The left panel of the figure shows the results obtained using the sum of the age and rs-fMRI data as the input, whereas the right panel shows the output when using only rs-fMRI data as the input. In each model, linear regression was performed using the least-squares method, and the shaded areas indicated 95% confidence intervals. Pearson's correlation and coefficient of determination are listed in the order of LASSO and cGCN-LSTM in the upper right corner. The asterisk symbols added to the correlation coefficients indicate $p<0.01$ when there are two, and $p<0.05$, when there is one.

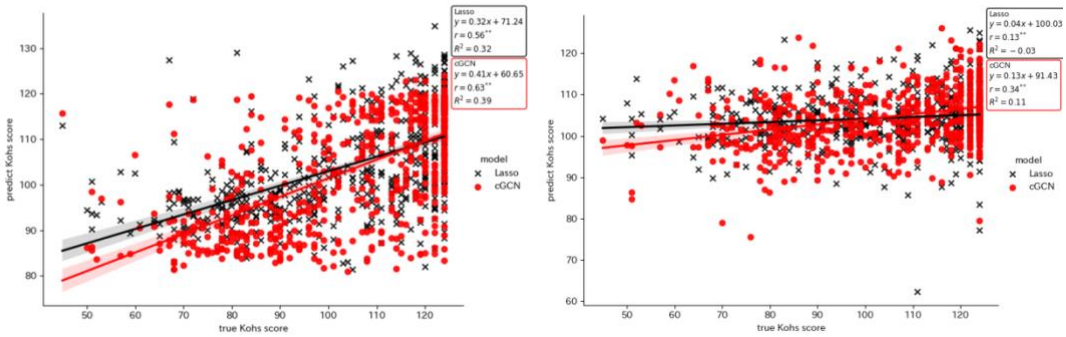

Figure 2. Prediction results of the Kohs block-design test scores. The horizontal axis represents the observed scores and the vertical axis denotes the predicted scores. The left side of the figure corresponds to the sum of age and rs-FC data as input, while the right side of the figure is based solely on rs-FC data input.

The model with both rs-fMRI data and age as inputs recorded a correlation coefficient of 0.63 for the cGCN-LSTM and 0.56 for the LASSO regression model on the Kohs test score. The cGCN-LSTM regression model outperformed the LASSO regression model; however, the difference between the models was marginal. However, when age was removed and only the rs-fMRI data were input, we found a significant deterioration in accuracy in the LASSO regression model compared to cGCN-LSTM, as the correlation coefficient for the cGCN-LSTM was 0.34 for the Kohs test score and 0.13 for the LASSO. This confirms the finding of Omidvarnia et al., 2023, that the LASSO results for rs-FC data had poorer cognitive predictive power relative to individual basic phenotype features. In comparison, the drop in the accuracy of resting-state FCs using cGCN-LSTM was small and captured the characteristics of resting-state FCs. Thus, the results indicate that depending on the choice of model, there is still potential for predicting cognitive ability using rs-FC data.

3.2 Important ROIs

Table 1 and Figure 3 show the decrease in accuracy for each ROI, the name of the ROI, the resting-state network to which the ROI belongs, and its importance rank in the age regression as applied to the trained cGCN-LSTM model. To test whether the

model can predict the covariate of age, age alone was also predicted using the model (Supplementary Materials, Figure B). Interestingly, the results showed a Spearman correlation of -0.0216 between the Kohs block-design test score and age, which was not significant. In Table 1, the rightmost column represents the ROI ranking in the age regression, with the top 20 rankings in italics.

It is now clear that ROIs have been extracted from various intrinsic networks, and some of them, such as those containing the left Heschl's gyrus (Heschl_L) and right anterior cingulate cortex (Cingulum_Ant_R), contribute the most to age estimation. Other extracted ROIs, such as those containing the right medial orbitofrontal cortex (Frontal_Med_Orb_R), Vermis 4 and 5 (Vermis_4_5), and Right Cerebellum 6 (Cerebelum_6_R), occupied low ranking positions in age estimation, despite its importance in Kohs test score prediction.

Table 1. Important ROIs for the prediction of Kohs block-design test scores. From left to right, the importance rank in score prediction, the decreasing range of Pearson's correlation coefficient, the name of the ROI, its attribution to a predefined intrinsic functional network in AAL, and its rank in age regression; the latter rank is marked in italics if within the top 20.

rank	reduction in R value	ROI	Intrinsic functional network	Rank(age prediction)
1	*-0.04029*	*Heschl_L*	*auditory*	*2*
2	-0.03715	Frontal_Med_Orb_R	DMN	107
3	-0.03526	Vermis_4_5	CN	116
4	*-0.0337*	*Cingulum_Ant_R*	*DMN/SN*	*1*
5	*-0.03355*	*Cuneus_R*	*VN*	*10*
6	-0.03247	Cerebelum_6_R	SN	67
7	-0.03191	Olfactory_R	SMN	28
8	*-0.03186*	*Vermis_9*	*CN*	*6*
9	-0.03132	Cuneus_L	VN	111
10	-0.03039	Temporal_Pole_Mid_L	DMN	41
11	-0.03022	Cerebelum_3_R	*CN*	13
12	-0.0299	Occipital_Mid_L	VN	56
13	-0.02981	Angular_R	DMN	84

14	-0.02977	Cerebelum_Crus2_R	EN	52
15	-0.02921	Rolandic_Oper_L	DAN/SMN	60
16	*-0.02912*	*Temporal_Pole_Mid_R*	*DMN*	*12*
17	-0.02908	Pallidum_L	subcortical	53
18	-0.02906	Temporal_Mid_R	DMN	102
19	-0.02896	Pallidum_R	subcortical	106
20	-0.02871	Amygdala_L	subcortical	32

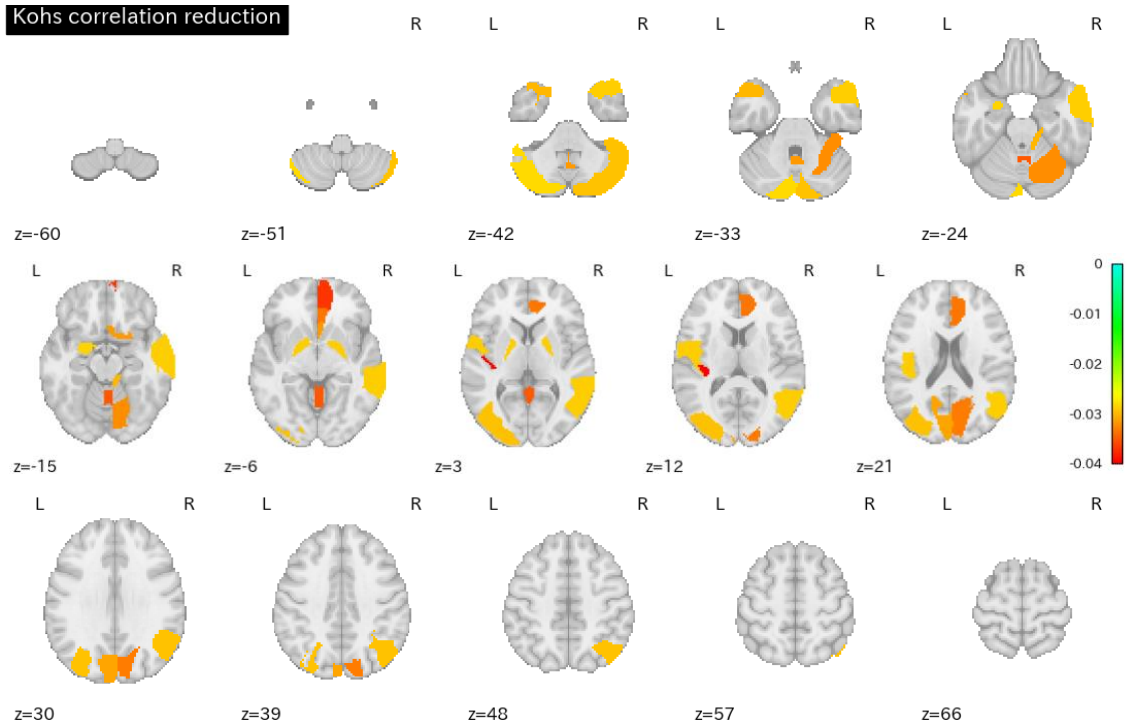

Figure 3. Visualization of important ROIs for the prediction of Kohs block-design test scores. Visualization was performed for the top 20. (Slices at MNI coordinates z=-60, -51, -42, -33,-24, -15, -6, 3, 12, 21, 30, 39, 48, 57, 66) The python package nilearn was used to create the figures.

The results of leave-two-out occlusion are shown in Figure 4. For a total of 6786 edges in the two ROI selections, we visualized 100 edges that were particularly important using the occlusion method. The left panel shows the edges grouped by brain structure, and the right panel shows the edges grouped by functional network. The figure indicates that the interconnections between the temporal lobe, frontal lobe, and cerebellum are critical for score prediction. Interestingly, significant interconnections between specific ROIs in the auditory network and the DMN are also found. It has also

been confirmed that the salience network (SN), executive network (EN), and visual network (VN) have key links.

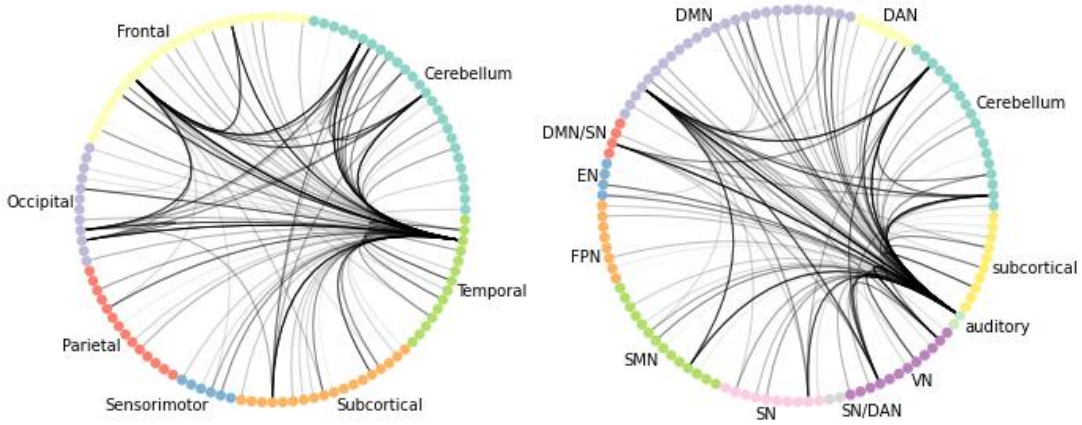

Figure 4. The most important region pairs (edges) for the prediction of Kohs block-design test scores and their relationship to the intrinsic networks. The visualization was made by using a Python library, nxviz (https://ericmjl.github.io/nxviz/)

4. Discussion

4.1 ROI and Networks

When focusing on the crucial ROIs and networks in the predictive model of the Kohs block-design test, whose scores declined with age, it was again confirmed that they were mentioned (Rozencwajg, 1991) in relation to general cognitive function. In particular, the fact that the DMN regions were extracted in this study confirms that this network is central to aging (Hafkemeijer et al., 2012; Hohenfeld et al., 2018). Furthermore, this study identified the cerebellum as an important brain region for predicting cognition-related ratings. Previous longitudinal MRI studies have shown that the cerebellum and the hippocampus have higher rates of volume loss in older adults (Raz et al., 2005). In terms of function, the cerebellum is assigned the role of high-speed information processing and modification of motor function in response to sensory and perceptual feedback and is considered to be a critical region in perceptual and motor tasks (Eckert et al., 2010). In particular, the cognitive function test used in

this study is believed to reflect, to some extent, motor processing ability along with processing speed, as the faster a person can answer the test, the higher the score. Considering the characteristics of this test, it is assumed that the information processing function of the cerebellum may be important. It should be further noted that only the DMN and cerebellum listed here contain some significant within-network connectivity, but overall, between-network connectivity overwhelmingly contributes to the prediction, which, coupled with the fact that important areas are distributed across the whole brain, requires further scrutiny.

This also raises the question of interpreting the importance of the VN in score prediction. Interestingly, Gao et al., 2020, who used rs-fMRI to predict processing speed (PS) in older adults, noted that the fast PS group showed higher intra-network connectivity within each of the motor and visual networks, but lower connectivity between the two networks, compared to the slow PS group. The results of our study showed an increase in the number of important connections from the nodes of the occipital lobe and VN in the score evaluation compared with age prediction (Supplementary Materials: Table A and Figure C), which at first glance appears to be consistent with the results of Gao et al., 2020. Certainly, in the task of aligning blocks while looking at a sample, it is possible that higher visual processing ability may have been more advantageous in terms of earning Kohs test scores. However, as noted earlier, the important FC within the network is limited to the DMN and cerebellar network and is not found in the VN.

4.2 cGCN-LSTM and Leave-two-out occlusion

As noted, a graph structure with group resting-state FC shows the possibility of successfully capturing the characteristics of functional networks. However, in the model with rs-fMRI and age as simultaneous inputs, the correlation coefficient of the LASSO regression model was 0.56 and that of the cGCN regression model was 0.63, with the latter outperforming the former. This difference was greatly magnified when age was removed as a factor, with a correlation coefficient of 0.13 for the LASSO regression model and 0.34 for the cGCN regression model when only rs-FC data were

input. It should be noted that Omidvarnia et al., 2023, reported that rs-FC plus age has predictive power for cognitive ability test scores but that modeling with rs-FC alone is much less accurate. However, unlike in this previous study, when a graph neural network (cGCN) is followed by a recurrent deep learning model (LSTM), i.e., cGCH-LSTM, the drop in accuracy is smaller than that of other algorithms.

One of the reasons for the lower accuracy in the LASSO regression model is its inability to capture the characteristics of time-series changes. In LASSO regression, FCS is used as input, but it is solely the sum of connection strengths above a threshold, which is a generalization of weighted order centrality. Therefore, it is important as a measure of connection weights between brain regions; however, it includes neither the functional and structural distances between ROIs nor time series information. Therefore, the FCS may have less information to guarantee the precision of regression modeling.

In contrast, the proposed cGCN-LSTM can fully utilize the following three advantages of the original cGCN. i) The same weights can be used for all subjects by applying a mask using group-averaged FC, thereby accelerating and simplifying learning. ii) We can take advantage of the selective use of features from ROIs that are functionally rather than structurally close to each other. iii) The parallelization of each time series in the cGCN, originally a discriminative model for patients with autism, boasts high accuracy even in a small number of frames compared with convolutional recurrent neural network (convRNN) models. Furthermore, as in the present study, it provides a foundation for a certain level of performance in regression problems, which is applied to cognitive decline or aging due to changes in functional connectivity. In this study, instead of averaging each time series prior to the final softmax layer, we could also obtain a new representation with the mean of the parallel convolutional series by introducing a fully connected layer to add LSTM at the end of the model. These are the advantages of our cGCN-LSTM model, which retains sufficient explanatory power even when the model is based only on rs-FC. Moreover, depending on further improvements, it may be possible to predict with even higher accuracy which brain regions contribute the most to a particular cognitive behavior from non-task-based resting-state fMRI data.

Regions that function only during a task and affect its performance can only be precisely determined using task-based fMRI experiments. However, the two-edge occlusion proposed in this study not only predicts task performance without requiring the relevant task in the scanning, but also evaluates which interregional relations contribute to the participant's activity. Such a task-free but task-related domain assessment is possible because cGCN-LSTM can predict cognitive test scores even when confounding factors such as age are excluded.

4.3 Limitations and Future perspectives

This section addresses the limitations and future challenges of this study. One limitation of this model is that a fixed number of nearest-neighbor areas (five in this study) were selected for each ROI and convolution was performed. Although this contributed to computational efficiency, it also created certain restrictions that made the graph structure potentially underoptimized. In addition, because of this restriction, when inference was performed on new data, the graph structure at the time of training was reused, which might not have captured the changes in FC between subjects. Although the prediction results showed a sufficiently significant correlation, the scores of the Kohs block-design test did not provide a very high prediction accuracy (0.34), and further improvement is needed as it would affect the interpretation of the model and ROIs. The unexpectedly small influence of the prefrontal cortex on the model may be partly due to the lack of precision. To improve the accuracy, it may be important to adopt a different data format. For example, recent studies have shown that FC is not stationary, but varies with time, called dynamic FC (dFC). Further improvements can be expected using a sliding window approach in dFC to select relevant ROIs according to the time-series changes in FC. This can be easily imagined from the poor results of cGCN-LSTM (Supplementary Materials, Figure B) compared with age prediction using dFC (Minowa et al., 2022).

Furthermore, because there was a correlation between the scores of Koh's test and age in this study, additional age prediction was executed to subtract brain regions that change with age from the relevant brain regions in the cognitive function test

prediction. However, this also requires further verification, as it is expected that there would be some brain areas excluded from consideration where these factors change in a coordinated manner. Furthermore, by using the occlusion method, it is possible to search for ROIs (vertices) and their pairs (edges) that have a large impact on the predicted values. However, even if the amount of impact is known, the causal relationship must be interpreted by the researchers themselves, and a new method to objectively evaluate this relationship is needed.

Despite these undeniable shortcomings, we were able to build a regression model worthy of proposal using a deep learning model called cGCN-LSTM. We were able to predict the scores of the offline Kohs block-design test using only the rs-FC data of 695 healthy subjects. This model and the leave-two-out occlusion allowed us to identify the regions and networks involved in further task-based fMRI experiments. Our methodology has the potential to make the design of task fMRI experiments more rational and accurate before planning and conducting actual scans.

5. References

Abraham, A., Pedregosa, F., Eickenberg, M., Gervais, P., Mueller, A., Kossaifi, J., Gramfort, A., Thirion, B., Varoquaux, G. (2014). Machine learning for neuroimaging with scikit-learn. Frontiers in Neuroinformatics, 8.

https://doi.org/10.3389/fninf.2014.00014

Buckner, R.L., Sepulcre, J., Talukdar, T., Krienen, F.M., Liu, H., Hedden, T., Andrews-Hanna, J.R., Sperling, R.A., Johnson, K.A. (2009). Cortical Hubs Revealed by Intrinsic Functional Connectivity: Mapping, Assessment of Stability, and Relation to Alzheimer's Disease. Journal of Neuroscience, 29 (6) 1860-1873

https://doi.org/10.1523/JNEUROSCI.5062-08.2009

Craddock, C., Sikka, S., Cheung, B., Khanuja, R., Ghosh, S.S., Yan, C., Li, Q., Lurie,D., Vogelstein, J., Burns, R., Colcombe, S., Mennes, M., Kelly, C., Di Martino, A.,

Castellanos, F.X., Milham, M. (2013). Towards Automated Analysis of Connectomes: The Configurable Pipeline for the Analysis of Connectomes (C-PAC). Frontiers in Neuroinformatics. Conference Abstract: Neuroinformatics 2013.

https://doi.org/10.3389/conf.fninf.2013.09.00042

De Luca, M., Beckmann, C., De Stefano, N., Matthews, P., & Smith, S. (2006). FMRI resting state networks define distinct modes of long-distance interactions in the human brain. NeuroImage, 29(4), 1359-1367.

https://doi.org/10.1016/j.neuroimage.2005.08.035

Eckert, M., Noam, K., Roberts, D., Calhoun, V., Harris, K. (2014). Age-related changes in processing speed: unique contributions of cerebellar and prefrontal cortex. Frontiers in Human Neuroscience, 8.

https://www.frontiersin.org/articles/10.3389/neuro.09.010.2010

Gao, M., Wong, C. H., Huang, H., Shao, R., Huang, R., Chan, C. C., & Lee, T. M. (2020). Connectome-based models can predict processing speed in older adults. NeuroImage, 223, 117290.

https://doi.org/10.1016/j.neuroimage.2020.117290

Hafkemeijer, A., van der Grond, J., & Rombouts, S. A. (2012). Imaging the default mode network in aging and dementia. Biochimica et Biophysica Acta (BBA) - Molecular Basis of Disease, 1822(3), 431-441.

https://doi.org/10.1016/j.bbadis.2011.07.008

Hanik, M., Demirtaş, M.A., Gharsallaoui, M.A., Rekik, I. (2022). Predicting cognitive scores with graph neural networks through sample selection learning. Brain Imaging

and Behavior 16, 1123–1138.

https://doi.org/10.1007/s11682-021-00585-7

Hohenfeld, C., Werner, C. J., & Reetz, K. (2018). Resting-state connectivity in neurodegenerative disorders: Is there potential for an imaging biomarker? NeuroImage: Clinical, 18, 849-870.

https://doi.org/10.1016/j.nicl.2018.03.013

Kohs, S. C. (1920). The Block-Design Tests. Journal of Experimental Psychology, 3(5), 357–376.

https://doi.org/10.1037/h0074466

Li, Q., Dong, C., Liu, T., Chen, X., Perry, A., Jiang, J., Cheng, J., Niu, H., Kochan, N. A., Brodaty, H., Sachdev, P. S., Wen, W. (2020). Longitudinal Changes in Whole-Brain Functional Connectivity Strength Patterns and the Relationship With the Global Cognitive Decline in Older Adults. Frontiers in Aging Neuroscience, 12.

https://www.frontiersin.org/articles/10.3389/fnagi.2020.00071

Meskaldji, D., Preti, M. G., Bolton, T. A., Montandon, M., Rodriguez, C., Morgenthaler, S., Giannakopoulos, P., Haller, S., & Van De Ville, D. (2016a). Predicting individual scores from resting state fMRI using partial least squares regression. IEEE 13th International Symposium on Biomedical Imaging (ISBI), Prague, Czech Republic, 1311-1314

https://doi.org/10.1109/ISBI.2016.7493508

Meskaldji, D., Preti, M. G., Bolton, T. A., Montandon, M., Rodriguez, C., Morgenthaler, S., Giannakopoulos, P., Haller, S., & Van De Ville, D. (2016b). Prediction of long-term

memory scores in MCI based on resting-state fMRI. NeuroImage: Clinical, 12, 785-795. https://doi.org/10.1016/j.nicl.2016.10.004

Minowa, Y., Onoda, K., Takamura, M., Yamaguchi, S., Okamoto, N., & Akama, H. (2022). Comparing Deep Learning Models for Age Prediction Based on the Resting State fMRI Dataset from the "Brain Dock" Service in Japan. bioRxiv, 2022.08.14.503923.

https://doi.org/10.1101/2022.08.14.503923

Omidvarnia, A., Sasse, L., Larabi, D.I., Raimondo, F., Hoffstaedter, F., Kasper, J., Dukart, J., Petersen, M., Cheng, B., Thomalla, G., Eickhoff, S.B., & Patil, K. R. (2023). Is resting state fMRI better than individual characteristics at predicting cognition? bioRxiv 2023.02.18.529076.

https://doi.org/10.1101/2023.02.18.529076

Raz, N., Lindenberger, U., Rodrigue, K.M., Kennedy, K. M., Head, D., Williamson, A., Dahle, C., Gerstorf, D., Acker, J. D. (2005). Regional Brain Changes in Aging Healthy Adults: General Trends, Individual Differences and Modifiers, Cerebral Cortex, 15(11):1676–1689,

https://doi.org/10.1093/cercor/bhi044

Rozencwajg, P. (1991). Analysis of Problem Solving Strategies on the Kohs Block Design Test, European Journal of Psychology of Education, 6(1):73-88.

https://doi.org/10.1007/BF03173149

Tzourio-Mazoyer, N., Landeau, B., Papathanassiou, D., Crivello, F., Etard, O., Delcroix, N., Mazoyer, B., & Joliot, M. (2002). Automated Anatomical Labeling of Activations in SPM Using a Macroscopic Anatomical Parcellation of the MNI MRI Single-Subject

Brain. NeuroImage, 15(1), 273-289.

https://doi.org/10.1006/nimg.2001.0978

Wang, L., Li, K., Hu, X. P. (2021). Graph convolutional network for fMRI analysis based on connectivity neighborhood. Network Neuroscience, 5(1):83–95.

https://doi.org/10.1162/netn_a_00171

Yoshida, K., Shimizu, Y., Yoshimoto, J., Takamura, M., Okada, G., Okamoto, Y., Yamawaki, S., & Doya, K. (2017). Prediction of clinical depression scores and detection of changes in whole-brain using resting-state functional MRI data with partial least squares regression. PLOS ONE, 12(7), e0179638.

https://doi.org/10.1371/journal.pone.0179638

6. Supplementary Materials

Layer (type)	Output Shape	Param #	Connected to
points (InputLayer)	(None, 140, 116, 2)	0	
graph (InputLayer)	(116, 5)	0	
lambda_1 (Lambda)	(None, 116, 5)	0	graph[0][0] points[0][0]
lambda_2 (Lambda)	(None, 140, 116, 5, 4)	0	points[0][0] lambda_1[0][0]
time_distributed_1 (TimeDistributed)	(None, 140, 116, 5, 8)	40	lambda_2[0][0]
time_distributed_2 (TimeDistributed)	(None, 140, 116, 5, 8)	0	time_distributed_1[0][0]
time_distributed_3 (TimeDistributed)	(None, 140, 116, 1, 8)	0	time_distributed_2[0][0]
lambda_4 (Lambda)	(None, 116, 5)	0	graph[0][0] time_distributed_3[0][0]
lambda_5 (Lambda)	(None, 140, 116, 5, 16)	0	time_distributed_3[0][0] lambda_4[0][0]
time_distributed_4 (TimeDistributed)	(None, 140, 116, 5, 8)	136	lambda_5[0][0]
time_distributed_5 (TimeDistributed)	(None, 140, 116, 5, 8)	0	time_distributed_4[0][0]
time_distributed_6 (TimeDistributed)	(None, 140, 116, 1, 8)	0	time_distributed_5[0][0]
lambda_7 (Lambda)	(None, 116, 5)	0	graph[0][0] time_distributed_6[0][0]
lambda_8 (Lambda)	(None, 140, 116, 5, 16)	0	time_distributed_6[0][0] lambda_7[0][0]
time_distributed_7 (TimeDistributed)	(None, 140, 116, 5, 8)	136	lambda_8[0][0]
time_distributed_8 (TimeDistributed)	(None, 140, 116, 5, 8)	0	time_distributed_7[0][0]
time_distributed_9 (TimeDistributed)	(None, 140, 116, 1, 8)	0	time_distributed_8[0][0]
lambda_10 (Lambda)	(None, 116, 5)	0	graph[0][0] time_distributed_9[0][0]
lambda_11 (Lambda)	(None, 140, 116, 5, 16)	0	time_distributed_9[0][0] lambda_10[0][0]
time_distributed_10 (TimeDistributed)	(None, 140, 116, 5, 16)	272	lambda_11[0][0]
time_distributed_11 (TimeDistributed)	(None, 140, 116, 5, 16)	0	time_distributed_10[0][0]
time_distributed_12 (TimeDistributed)	(None, 140, 116, 1, 16)	0	time_distributed_11[0][0]
lambda_13 (Lambda)	(None, 140, 116, 1, 40)	0	time_distributed_3[0][0] time_distributed_6[0][0] time_distributed_9[0][0] time_distributed_12[0][0]
lambda_14 (Lambda)	(None, 116, 5)	0	graph[0][0] lambda_13[0][0]
lambda_15 (Lambda)	(None, 140, 116, 5, 80)	0	lambda_13[0][0] lambda_14[0][0]
time_distributed_13 (TimeDistributed)	(None, 140, 116, 5, 32)	2592	lambda_15[0][0]
time_distributed_14 (TimeDistributed)	(None, 140, 116, 5, 32)	0	time_distributed_13[0][0]
time_distributed_15 (TimeDistributed)	(None, 140, 116, 1, 32)	0	time_distributed_14[0][0]
time_distributed_16 (TimeDistributed)	(None, 140, 116, 1, 32)	0	time_distributed_15[0][0]
conv_lst_m2d_1 (ConvLSTM2D)	(None, 140, 116, 1, 32)	8320	time_distributed_16[0][0]
time_distributed_17 (TimeDistributed)	(None, 140, 116, 1, 32)	128	conv_lst_m2d_1[0][0]
time_distributed_18 (TimeDistributed)	(None, 140, 116, 1, 32)	0	time_distributed_17[0][0]
time_distributed_19 (TimeDistributed)	(None, 140, 3712)	0	time_distributed_18[0][0]
time_distributed_20 (TimeDistributed)	(None, 140, 3712)	0	time_distributed_19[0][0]
time_distributed_21 (TimeDistributed)	(None, 140, 1)	3713	time_distributed_20[0][0]
lstm_1 (LSTM)	(None, 116)	54752	time_distributed_21[0][0]
dense_2 (Dense)	(None, 1)	117	lstm_1[0][0]

Total params: 70,206
Trainable params: 70,142
Non-trainable params: 64

Figure A. Procedures with layer, shape, parameter and connection setting of our cGCN-LSTM.

LSTM is added in place of time series averages.

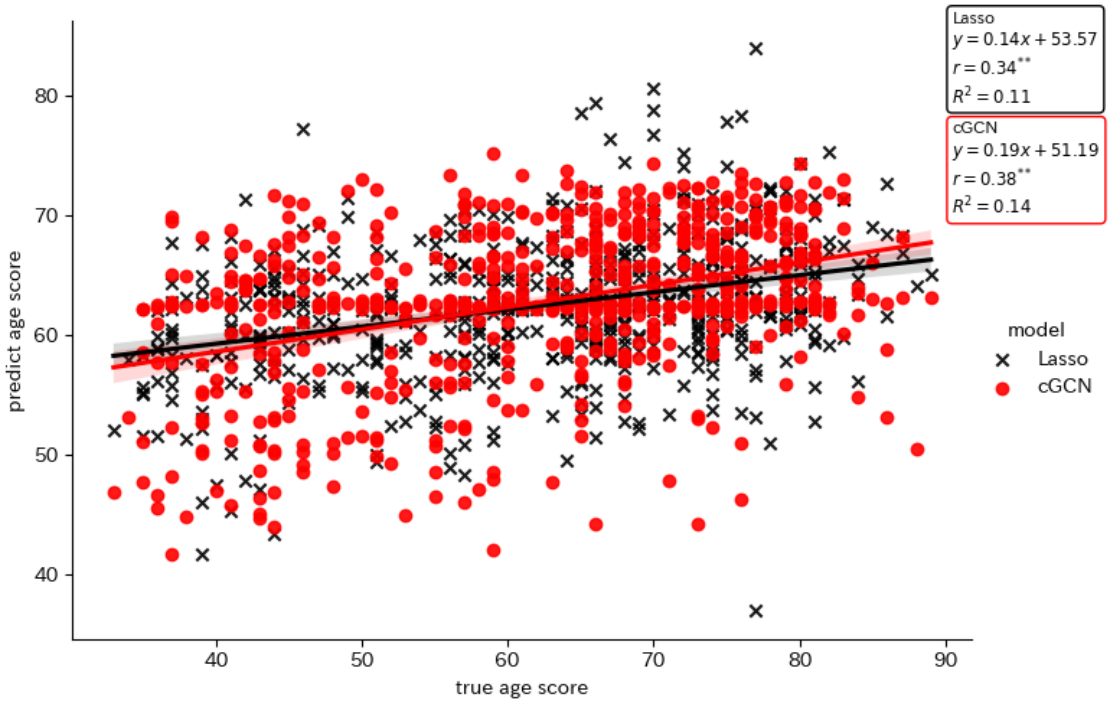

Figure B. Results of age prediction. The horizontal axis represents the observed ages and the vertical axis denotes the predicted ages.

Table A. Important ROIs for the age prediction

rank	r reduction	ROI	network
1	-0.033968253	Cingulum_Ant_R	DMN/SN
2	-0.032056298	Heschl_L	auditory
3	-0.023317771	Cerebelum_3_L	CN
4	-0.023036771	Cerebelum_9_R	DMN
5	-0.020415184	Temporal_Sup_R	DAN
6	-0.019949884	Vermis_9	CN
7	-0.019709637	Temporal_Pole_Sup_R	SN
8	-0.019566773	Lingual_R	VN
9	-0.018090764	Cingulum_Post_R	DMN
10	-0.017188389	Cuneus_R	VN
11	-0.015721649	Vermis_1_2	CN
12	-0.015358761	Temporal_Pole_Mid_R	DMN
13	-0.015281032	Cerebelum_3_R	CN
14	-0.015240625	Frontal_Med_Orb_L	DMN

15	-0.015224133	ParaHippocampal_R	DMN
16	-0.014870114	Temporal_Sup_L	DAN
17	-0.014671268	Frontal_Mid_Orb_L	FPN
18	-0.014628147	Temporal_Inf_L	DAN
19	-0.014407255	Frontal_Mid_R	SN/FPN
20	-0.02871	Amygdala_L	subcortical

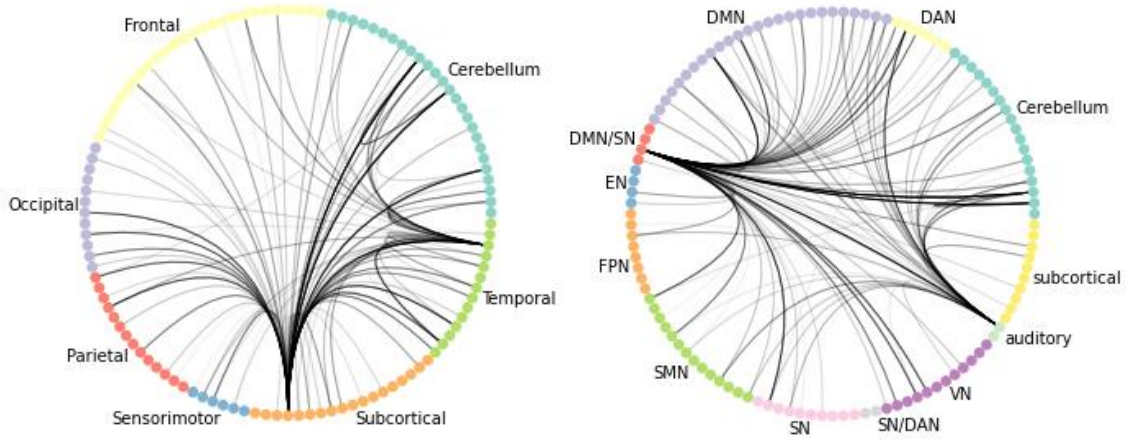

Figure C. The most important region pairs (edges) for age prediction and their relationship to the intrinsic networks. The visualization was made using a Python library, nxviz (https://ericmjl.github.io/nxviz/)

Note:

This paper is an abstract of the master's thesis of the first author, who is now an alumnus of the Tokyo Institute of Technology, Japan.

Data availability

Limited phenotypic data (subject ID, age, and sex) and inputs (ROI mean time-series data based on the AAL and HO atlases only) of the neural networks generated for this study are available with all Python code for data analysis at https://github.com/yutads/shimane. However, functional MRI images are not available to the public online because of the conditions for approval of the study set by institutional review boards. The scripts for computing the cGCN-LSTM are available at https://github.com/tokuotsu/cGCN-LSTM.git.

Funding

This work was supported by the Japan Society for the Promotion of Science (Grant No. JP15K12425).

Competing interests

The authors declare that this study was conducted in the absence of any commercial or financial relationships that could be construed as potential conflicts of interest.

Acknowledgements

The authors would like to thank Editage (www.editage.jp) for English language editing.